



HAL
open science

The Added Value of Longitudinal Imaging for Preclinical In vivo Efficacy Testing of Therapeutic Compounds against Cerebral Cryptococcosis

Liesbeth Vanherp, Jennifer Poelmans, Amy Hillen, Guilhem Janbon, Matthias Brock, Katrien Lagrou, Greetje Vande Velde, Uwe Himmelreich

► **To cite this version:**

Liesbeth Vanherp, Jennifer Poelmans, Amy Hillen, Guilhem Janbon, Matthias Brock, et al.. The Added Value of Longitudinal Imaging for Preclinical In vivo Efficacy Testing of Therapeutic Compounds against Cerebral Cryptococcosis. *Antimicrobial Agents and Chemotherapy*, 2020, 64 (7), pp.e00070-20. 10.1128/AAC.00070-20 . pasteur-02652024

HAL Id: pasteur-02652024

<https://pasteur.hal.science/pasteur-02652024>

Submitted on 29 May 2020

HAL is a multi-disciplinary open access archive for the deposit and dissemination of scientific research documents, whether they are published or not. The documents may come from teaching and research institutions in France or abroad, or from public or private research centers.

L'archive ouverte pluridisciplinaire **HAL**, est destinée au dépôt et à la diffusion de documents scientifiques de niveau recherche, publiés ou non, émanant des établissements d'enseignement et de recherche français ou étrangers, des laboratoires publics ou privés.

1 **Title page**

2 **Title**

3 The Added Value of Longitudinal Imaging for Preclinical *In vivo* Efficacy Testing of
4 Therapeutic Compounds against Cerebral Cryptococcosis

5 **Running title**

6 *In vivo* imaging of anticytotoxic treatment in mice

7 **Authors**

8 Liesbeth Vanherp^{a,b}, Jennifer Poelmans^{a,b,°}, Amy Hillen^{a,b,◇}, Guilhem Janbon^c,
9 Matthias Brock^d, Katrien Lagrou^{e,f}, Greetje Vande Velde^{a,b,#,*}, Uwe Himmelreich^{a,b,*}

10 # Address correspondence to Greetje Vande Velde,
11 greetje.vandavelde@kuleuven.be

12 * G.V.V. and U.H. contributed equally to this work

13 **Affiliations**

14 ^a Biomedical MRI, Department of Imaging and Pathology, KU Leuven, Leuven,
15 Belgium

16 ^b Molecular Small Animal Imaging Center (MoSAIC), KU Leuven, Leuven, Belgium

17 ^c RNA Biology of Fungal Pathogens, Department of Mycology, Pasteur Institute,
18 Paris, France

19 ^d Fungal Biology Group, School of Life Sciences, University of Nottingham,
20 Nottingham, United Kingdom

21 ^e Laboratory of Clinical Bacteriology and Mycology, Department of Microbiology,
22 Immunology and Transplantation, KU Leuven, Leuven, Belgium.

23 ^f National Reference Centre for Mycosis, Department of Laboratory Medicine,
24 University Hospitals Leuven, Leuven, Belgium

25 ^o Present address: The Janssen Pharmaceutical Companies of Johnson & Johnson,
26 Beerse, Belgium

27 [◇] Present address: Department of Cell and Molecular Biology (CMB), Karolinska
28 Institutet, Stockholm, Sweden

29 **Abstract**

30 Brain infections with *Cryptococcus neoformans* are associated with significant
31 morbidity and mortality. Cryptococcosis typically presents as meningoencephalitis or
32 fungal mass lesions called cryptococcomas. Despite frequent *in vitro* discoveries of
33 promising novel antifungals, the clinical need for drugs that can more efficiently treat
34 these brain infections remains. A crucial step in drug development is the evaluation of
35 *in vivo* drug efficacy in animal models. This mainly relies on survival studies or post-
36 mortem analyses in large groups of animals, but these techniques only provide
37 information on specific organs of interest at predefined time points. In this proof-of-
38 concept study, we validated the use of non-invasive preclinical imaging to obtain
39 longitudinal information on the therapeutic efficacy of amphotericin B or fluconazole
40 monotherapy in meningoencephalitis and cryptococcoma mouse models.
41 Bioluminescence imaging (BLI) enabled the rapid *in vitro* and *in vivo* evaluation of
42 drug efficacy while complementary high-resolution anatomical information obtained
43 by magnetic resonance imaging (MRI) of the brain allowed a precise assessment of
44 the extent of infection and lesion growth rates. We demonstrated a good correlation
45 between both imaging readouts and the fungal burden in various organs. Moreover,
46 we identified potential pitfalls associated with the interpretation of therapeutic efficacy
47 based solely on post-mortem studies, demonstrating the added value of this non-
48 invasive dual imaging approach compared to standard mortality curves or fungal load
49 endpoints. This novel preclinical imaging platform provides insights in the dynamic
50 aspects of the therapeutic response and facilitates a more efficient and accurate
51 translation of promising antifungal compounds from bench to bedside.

52 **Introduction**

53 Fungal infections of the central nervous system (CNS) are generally associated with
54 high mortality rates and poor prognosis (1). The group of patients at risk for
55 contracting these opportunistic infections has grown due to the increased prevalence
56 of disease-induced or treatment-related immunosuppression (2). Of the few fungal
57 species able to infect the brain, *Cryptococcus neoformans* is worldwide one of the
58 most common causative organisms (2). It infects mainly HIV-patients, but also
59 persons with underlying medical conditions or receiving immunosuppressive
60 treatment, and occasionally immunocompetent individuals (3). Cryptococcal infection
61 of the CNS arises after dissemination or reactivation of fungal cells that were initially
62 acquired through inhalation. Most frequently, the disease presents as a subacute
63 meningoencephalitis, with small accumulations of yeasts in the brain parenchyma (4,
64 5). More rarely, it causes mass lesions in the brain parenchyma, called
65 cryptococcomas (1). These occur more frequently in immunocompetent patients due
66 to the local containment of infection by the host response (6, 7).

67 Despite some recent progress in the development of novel antifungals, current
68 treatment for cerebral cryptococcosis still uses drugs that were developed several
69 decades ago (8, 9). The standard induction regimen combines the fungicidal polyene
70 amphotericin B (AMB) with 5-fluorocytosine (10, 11). However, these drugs are not
71 widely available and require intravenous administration and careful monitoring for
72 drug-related toxicity. For these reasons, they are sometimes replaced by the oral
73 drug fluconazole (FLC) in resource-limited settings, but monotherapy with this
74 fungistatic drug is less efficacious (12). Despite recent advances in optimizing
75 accessible combination therapies (13), the clinical need for effective, low-cost and
76 widely available anticryptococcal drugs with minimal toxicity remains high (14).

77 Although new candidate drugs are frequently reported following *in vitro* screenings,
78 only a very limited amount of these eventually reaches the clinic. For CNS infections,
79 the presence of the blood-brain barrier (BBB) poses an additional hurdle in drug
80 development. Even of the currently available antifungal compounds, only a few can
81 efficiently reach the brain tissue (15).

82 To ensure an optimal translation from bench to bedside, testing the *in vivo* efficacy of
83 a drug in animal models remains a crucial step as it allows studying the therapeutic
84 response in a complex yet controlled system (16). Mammalian models allow the
85 evaluation of therapy in the presence of an immune system and blood-brain barrier
86 that is comparable to humans, including their potential disease-related changes. In
87 murine models, response to antifungal treatment is frequently evaluated using
88 survival curves, post-mortem colony-forming unit (CFU) analysis of the fungal load or
89 histopathologic examination of the isolated organs (16, 17). However, these
90 techniques pose some challenges as they only provide single endpoint
91 measurements of the disease status and limited information about spatial distribution
92 of disease. When a temporal profile of drug efficacy is required, these studies rely on
93 large groups of animals in order to isolate specific organs at predefined time points.

94 More recently, non-invasive imaging techniques have been developed that allow
95 longitudinal evaluation of the fungal infection status or treatment response in
96 individual animals. Bioluminescence imaging (BLI) measures the light emitted from
97 the oxidation of a substrate by an enzyme such as *Gaussia* or firefly luciferase.
98 Numerous studies have shown and extensively validated that the measured signal is
99 proportional to the number of cells expressing the luciferase and their viability (18–
100 23), as intracellular ATP of living cells is essentially required for the light-emitting
101 reaction of the firefly luciferase (24). By genetically engineering fungi to express this

102 luciferase reporter gene, the *in vitro* activity of antifungal compounds (19, 23, 25) and
103 the temporal and spatial distribution of the infectious burden in living animals can be
104 monitored (23, 26–28). In this respect, treatment studies using animal models of
105 aspergillosis and candidiasis have shown a good correlation between traditional CFU
106 analysis of the fungal load and treatment effects observed in various organs by using
107 BLI (19, 26, 27, 29). Previously, we have developed and validated the use of a novel
108 bioluminescent *Cryptococcus neoformans* strain for tracking pathogen dissemination
109 from the lung to the brain (28). Hereby, we demonstrated a clear correlation between
110 the number of CFUs and the emitted light, both *in vitro* and *in vivo*. Furthermore,
111 magnetic resonance imaging (MRI) of the brain allowed a detailed analysis of the
112 spatial distribution of infectious foci. However, to date, preclinical imaging techniques
113 have not been used to monitor antifungal treatment efficacy against fungal infections
114 of the CNS, such as cryptococcosis.

115 In this study, we assessed the use of BLI for screening the *in vitro* efficacy of
116 antifungal compounds against *C. neoformans*. Secondly, we evaluated the
117 combination of whole-body BLI and brain MRI to non-invasively monitor *in vivo*
118 antifungal treatment efficacy with temporal and spatial resolution and validated this
119 against standard CFU endpoint measurements. To this end, we tested liposomal
120 AMB (L-AMB) or FLC monotherapy in murine models reflecting two distinct
121 presentations of cerebral cryptococcosis: (i) a standard model of cryptococcal
122 meningoencephalitis following disseminated disease and (ii) a model of a local
123 cryptococcoma. In both cases, the treatment was delayed until BLI revealed that
124 established disease was present. This late initiation of therapy was applied as it is
125 similar to the clinical setting in which patients often present with advanced infection
126 before being diagnosed. By obtaining longitudinal information on the dynamic

127 process of treatment response in individual animals, we aimed to demonstrate the
128 potential, validity and added value of using non-invasive imaging in preclinical drug
129 testing for fungal brain infections.

130 **Results**

131 ***In vitro* bioluminescence assays enable rapid real-time assessment of** 132 **fungicidal and fungistatic antifungal drug activity**

133 To validate the potential of BLI to follow-up antifungal effects on cryptococcal cells,
134 the bioluminescence emitted by *C. neoformans* reporter cells was measured *in vitro*
135 at several time points after addition of amphotericin B deoxycholate (AMB-d) and
136 fluconazole (FLC) (Fig. 1). The BLI signal intensity of the untreated cells highly
137 increased in the beginning (0-6h), followed by a stable signal measured at 8 and 24h
138 and a subsequent decline in aging cultures. After addition of AMB-d (0.1 mg/ml),
139 bioluminescence decreased to background levels within two hours, indicating a rapid
140 fungicidal effect of this drug at the tested concentration. Upon addition of the
141 fungistatic drug FLC (0.5 mg/ml), the emitted bioluminescence initially continuously
142 increased, but stagnated after 4 hours, followed by a decrease after 24 hours.

143 **AMB induces a transient increase in bioluminescence that is potentially** 144 **mediated by enhanced permeability for D-luciferin**

145 After confirming the ability to detect antifungal effects using bioluminescence, we
146 characterized the temporal profile of the bioluminescence signal in response to a
147 wide concentration range of antifungals using a similar *in vitro* set-up. At 8 and 26
148 hours after exposure, a dose-dependent decrease in bioluminescence was observed
149 for all tested concentrations of AMB-d and L-AMB, corresponding to its fungicidal
150 effect (Fig. 2A-B, Fig. S1). When using the fungistatic agent FLC, the
151 bioluminescence increased more slowly in cells exposed to higher concentrations
152 (Fig. 2C, Fig. S1). At 8 hours, we observed a dose-dependent reduction of
153 bioluminescence compared to the control.

154 Bioluminescence transiently increased immediately after the addition of AMB-d or L-
155 AMB, while a similar effect was not observed for FLC (Fig. 2, S1). Higher doses of
156 AMB induced a larger and more rapid increase, which was smaller and more delayed
157 for L-AMB compared to AMB-d.

158 We investigated potential explanations for this increased bioluminescence in parallel
159 experiments, using a *C. neoformans* strain with a fluorescent E2-Crimson reporter
160 gene under control of the same promoter. Addition of the antifungals induced only a
161 slight decrease in fluorescence, whereby the dose-dependent antifungal effect was
162 most notable for FLC (Fig. S2). We did not observe increased fluorescence upon
163 addition of the antifungals, indicating that a change in the expression levels of the
164 reporter gene was not the cause of the increased bioluminescence. Furthermore, we
165 found that none of the tested antifungals was auto-luminescent or auto-fluorescent in
166 water or Sabouraud medium (Fig. S3), nor caused luminescence in wild-type *C.*
167 *neoformans* cells (Fig. S4).

168 Since AMB affects the integrity of the cell membrane and induces transmembrane
169 channels (30, 31), we hypothesized that this transient bioluminescence increase
170 might be caused by enhanced permeability of the fungal cells for the substrate D-
171 luciferin (32). Exposure to natamycin, a polyene antifungal that does not permeabilize
172 the plasma membrane (33), led to a dose-dependent decrease in bioluminescence
173 corresponding to its antifungal effect (Fig. 2D, Fig. S1). Only at the highest
174 concentration tested (100 µg/ml), we observed a transient increase prior to this
175 decrease. Exposure to SDS, a surfactant leading to destruction of cell integrity and
176 cell death, induced a rapid and dose-dependent reduction of bioluminescence (Fig.
177 2E, Fig. S1).

178 **Whole-body BLI allows simultaneous evaluation of drug efficacy at multiple**
179 **body sites in a model of disseminated cryptococcosis**

180 We subsequently validated the use of BLI and MRI for *in vivo* evaluation of antifungal
181 treatment efficacy by using different treatment regimens in a standard model of
182 advanced cryptococcal meningoencephalitis following disseminated disease (Fig.
183 3A). After i.v. injection of cryptococci, control animals developed a progressive
184 infection in the brain and the abdomen, including the spleen and kidney region, as
185 previously described (28) (Fig. 4). The baseline infection status was assessed on day
186 3 and this identified an unsuccessful induction of infection in one animal of the FLC-
187 treated group. Treatment with L-AMB significantly reduced the infection in the
188 abdomen, while the bioluminescence from the brain was comparable to the control
189 group. We observed a higher brain and abdomen bioluminescence in L-AMB treated
190 animals than control animals specifically on day 4 p.i., when imaging was performed
191 less than three hours after injection of antifungals. Animals treated with FLC showed
192 a significant delay in the development of high brain signal intensity until day 6 p.i.,
193 after which the signal increased. The bioluminescence from the abdominal region
194 was reduced compared to the control group, except for one animal that presented
195 with a persistent hotspot in all images.

196 MR imaging of the brain showed that disease progression is associated with an
197 increase in the total lesion volume, number of brain lesions and average volume per
198 lesion (Fig. 5). L-AMB treatment induced a small reduction in the total lesion volume,
199 but not in the number of brain lesions or their average volume. The MRI on day 4 p.i.
200 did not show a difference between the L-AMB treated and control animals that could
201 explain the higher BLI signal intensity observed for the former group. Animals treated
202 with FLC presented with a significantly lower total lesion volume and a smaller

203 average lesion volume compared to untreated or L-AMB treated animals. This was
204 confirmed in lesion volume distributions obtained on day 6 (Fig. S5).

205 In agreement with the imaging results, CFU analysis showed that L-AMB led to a
206 large reduction of the fungal load in the spleen and kidneys, while having a limited
207 effect in the brain (Fig. 6). In comparison, FLC led to a larger reduction of the brain
208 fungal load but had a more limited effect in the spleen and kidney. Quantitative cross-
209 correlation of imaging results and CFU counts indicated that BLI results of the
210 abdomen correlated well with the fungal load in the spleen and kidneys (Fig. S6). In
211 the brain, the lesion volume quantified from the 3D MRI was highly correlated with
212 the fungal load. On day 7 p.i., we could not detect a significant correlation between
213 the BLI results and the brain fungal burden, mainly due to the limited differences in
214 the BLI signal. Nevertheless, we found that the BLI results on day 6 were predictive
215 for the fungal burden on day 7, as evidenced by their good correlation.

216 **BLI and MRI provide highly complementary information about the individual**
217 **response to systemic therapy in a cryptococcoma model**

218 In a second proof-of-concept study, we tested the combination of *in vivo* BLI and MRI
219 for monitoring treatment efficacy in a mouse model of a local cryptococcoma (Fig. 3
220 B). At baseline (day 3), established cryptococcomas were present in the mouse
221 brains, with detectable bioluminescence and hyperintense focal lesions on the MR
222 images (Fig. 7). The brain BLI signal intensity of untreated animals progressively
223 increased (Fig. 7 A, C) and was paralleled by an increase in the lesion volume on
224 MRI (Fig. 7 B, D). A single i.v. high dose of L-AMB showed no obvious treatment
225 success. In contrast, animals treated with FLC generally presented with lower
226 bioluminescence signal intensities and smaller brain lesions, indicating a response to
227 antifungal therapy. Daily i.p. injections with L-AMB led to large inter-animal variability

228 in the response. The animal with the smallest lesion at baseline showed low
229 bioluminescence and limited lesion growth on MRI. One animal showed a limited
230 increase in bioluminescence, while the lesion volume increased substantially. The
231 other two animals presented with a large increase in BLI signal, but this was not
232 associated with larger brain lesions on MRI. However, MRI indicated that the
233 infection was no longer confined to the induced lesion and had spread into the
234 ventricle or towards the forebrain. The same was observed for one animal in the
235 FLC-group. Histology confirmed that this presentation of the disease on MRI is
236 typically associated with presence of cryptococci in the ventricles (Fig. S7).

237 After the last imaging session on day 9, CFU analysis showed an approximate
238 tenfold reduction in the brain fungal load of most animals receiving daily L-AMB or
239 FLC, although this difference was not significant (Fig. 8A). Invasion of the lesion into
240 the ventricle was not associated with a higher fungal burden, except for one animal
241 where infection had also spread to the forebrain. The *in vivo* BLI results correlated
242 well with the fungal burden in the brain (Fig. 8B), and exclusion of the few animals
243 with ventricular involvement further strengthened this correlation. Furthermore, we
244 found good correspondence between fungal burden and lesion volume on MRI (Fig.
245 8C).

246 **Intracerebral amphotericin B treatment shows limited efficacy in the** 247 **cryptococcoma model**

248 Due to the limited antifungal effect observed in the cryptococcoma model upon
249 systemic treatment with L-AMB, we subsequently evaluated the efficacy of direct
250 intracerebral injection delivering L-AMB in the cryptococcoma, as this would bypass
251 the role of the blood-brain-barrier (BBB) in drug delivery (Fig. 3C). Similar to the
252 control group, the brain BLI signal intensity increased for most animals in the L-AMB

253 group, except for animal 1 and 2 that showed a stagnated BLI signal on day 10 (Fig.
254 9A, C). In contrast, the lesion volume increased for all animals (Fig. 9B, D). On some
255 MR images, a small hyperintensity could be seen inside the lesion due to the
256 injection. Its limited size compared to the whole lesion size could indicate that only
257 part of the lesion was effectively targeted. CFU analysis showed a small but
258 significant reduction in the fungal load, with limited variability within the group (Fig.
259 S8). Although animal 1 and 2 showed a response on BLI, their fungal burden and
260 lesion volume was similar to the other animals. This indicates that intracerebral
261 injection of L-AMB in this cryptococcoma model is not superior to intraperitoneal
262 delivery of the drug.

263 **Discussion**

264 In this work, we have demonstrated that BLI enables qualitative and quantitative
265 evaluation of the *in vitro* and *in vivo* therapeutic efficacy of antifungal compounds
266 against *C. neoformans*. MRI provided a complementary readout on treatment effects
267 by monitoring the spatial distribution and growth rate of lesions in the brain. Both BLI
268 and MRI results were in good agreement with CFU analysis, allowing a non-invasive
269 *in vivo* assessment of the fungal load. In contrast to single time point measurements
270 such as CFU analysis or histology, this novel approach provides information about
271 the temporal and spatial evolution of the infection and therapeutic response in living
272 animals and allows studying multiple infections sites simultaneously. Moreover,
273 longitudinal imaging is non-invasive and reduces the number of animals needed for
274 the preclinical evaluation of antifungal therapy as individual animals can be
275 monitored throughout the full disease and treatment process. Therefore, the
276 implementation of preclinical imaging can raise the ethical acceptance of *in vivo*
277 efficacy studies, which remain an essential step for the evaluation of novel
278 therapeutic compounds.

279 BLI enabled rapid real-time screening of *in vitro* antifungal drug efficacy with
280 distinction between fungistatic and fungicidal activity. The use of real-time imaging
281 techniques for determination of drug sensitivity and time-kill curves has the
282 advantage that plating of samples for CFU counting can be neglected and results are
283 obtained immediately (34). This makes BLI an interesting alternative for rapid real-
284 time *in vitro* assessment of antifungal activity, and multiplexing BLI with fluorescence
285 or dye-based approaches can provide additional validation of the results (19, 34). As
286 some drugs induced a temporal increase in bioluminescence, robust testing of the
287 antifungal effect should be done a broader time window to avoid measuring only

288 these difficult to interpret transient effects. Alterations in membrane permeability
289 causing an increased substrate influx are a possible contributor, and previous studies
290 have used luciferase reporters to assess cell permeabilization in bacteria (32).
291 Further study is warranted to investigate how this transient increase relates to the
292 complex mode of action of antifungals, and whether similar effects are also present
293 with other bioluminescent organisms.

294 Subsequently, we aimed to validate a combination of non-invasive optical and
295 anatomical imaging for *in vivo* evaluation of antifungal treatment efficacy in two
296 mouse models and compared these to standard endpoint measurements such as
297 CFU counts to quantify fungal load. Both BLI and MRI readouts correlated well with
298 the fungal burden in various organs, indicating that our dual imaging approach
299 represents a valuable non-invasive alternative, or at least compatible addition, to the
300 traditional post-mortem techniques. Even more so, our findings indicated that results
301 from endpoint analyses can lead to misinterpretation of treatment effects and showed
302 that these limitations can be overcome using non-invasive imaging. In the
303 disseminated disease model, the therapeutic response was variable throughout the
304 disease period, indicating that the selection of specific time points for fungal load
305 analysis and correct identification of infected body sites (such as brain versus kidney
306 infection) can have a large impact on conclusions about *in vivo* drug efficacy.
307 Furthermore, our approach qualitatively and quantitatively assessed the infection
308 status of individual animals prior to the start of treatment and identified animals in
309 which induction of infection had failed, which might be wrongly interpreted as
310 treatment success in single time point analyses. In addition, whole-body BLI allowed
311 simultaneous assessment of the antifungal efficacy in various organs, including
312 organs that were not in primary focus of this study. This contrasts techniques like

313 CFU counting or histology, where effects are only studied in predefined organs.
314 Hence, the implementation of this dual imaging approach in preclinical drug efficacy
315 testing for CNS infections allows a more efficient and more complete assessment of
316 the therapeutic effect than the standard techniques.

317 Overall, our BLI readouts correlated well to the current gold standard of CFU
318 analysis, but for correct interpretation of BLI results it remains important to realize
319 that several confounding factors may limit a direct translation from BLI signal to viable
320 fungal load. First, the localization of infection affects the amount of detectable light.
321 The BLI signal was higher when infection had spread to the ventricles and CSF
322 compared to deep-seated, localized cryptococcomas, although this was not
323 associated with an increased fungal load. Secondly, the bioluminescence reaction
324 using firefly luciferases requires the availability of D-luciferin and the cofactors O₂,
325 ATP and Mg²⁺. Especially in larger or necrotic lesions, the delivery of oxygen and the
326 substrate D-luciferin might be limited, leading to a lower signal intensity (22).
327 Changes in the BBB-integrity could also affect the permeability for D-luciferin (35).
328 Finally, we showed that some drugs may cause a transient BLI increase potentially
329 due to altered membrane permeability and luciferin uptake, which could result in
330 reduced correlation of the BLI signal with CFU counts. Our study illustrated that
331 performing *in vivo* experiments in this specific time window of transient effects may
332 lead to a transiently increased bioluminescence that is not necessarily related to an
333 increased fungal load.

334 The addition of MRI provided a valuable second readout on treatment efficacy by
335 monitoring with high spatial detail how antifungal treatment affects the growth rate
336 and spatial distribution of brain lesions and limits damage to the host brain. In the
337 meningoencephalitis model, MRI allowed the detailed analysis of the number of brain

338 lesions and their respective size and showed an excellent correlation with the fungal
339 load in the brain. Although MRI was able to demonstrate a slower growth rate of
340 lesions upon treatment, successful antifungal therapy will most likely not result in
341 rapid shrinkage of the lesion, as has also been shown in clinical MR studies (36). As
342 the hyperintense contrast on MRI is not specifically generated by viable fungi, the
343 result of antifungal treatment will likely show a delayed response on MRI, in contrast
344 to BLI where a direct effect on fungal cell viability can be observed. But, in contrast to
345 BLI, MRI does not require genetic modification of the fungal strain and is also
346 implemented in a clinical setting.

347 The highly complementary information obtained by the combination of BLI and MRI
348 can overcome the limitations of the individual imaging techniques. Our study showed
349 that this is extremely valuable for correct interpretation of results. The acquired
350 whole-body BLI images can be used to monitor and quantify the differential spatial
351 and temporal distribution of infection and treatment effects in multiple organs
352 simultaneously. BLI can guide additional anatomical imaging techniques towards
353 organs of interest to obtain a detailed 3D localization of the infectious foci. MRI can
354 provide an alternative readout on the infection status to validate the BLI results and
355 identify potential reasons for specific observations with BLI. As an example, MRI
356 showed the spatial distribution of infection towards the ventricles, or can detect
357 bleeding or scar tissue which may attenuate the emitted light. In this way, BLI and
358 MRI provide highly complementary information on different aspects of the therapeutic
359 response: the direct effect on viable fungal load (BLI) or on lesion growth and
360 damage to the host (MRI).

361 We have validated this novel imaging approach in two different animal models of
362 cryptococcosis that represent two distinct clinical presentations of the disease.

363 Treatment was generally less effective in the cryptococcoma model than the
364 meningoencephalitis model, most likely due to limited drug penetration in large
365 lesions. This corresponds to clinical case reports, where cryptococcomas are
366 typically difficult to treat and require prolonged antifungal treatment and sometimes
367 surgical resection (10, 37, 38). Moreover, meningoencephalitis models have a
368 demonstrated impairment of the BBB-integrity leading to more efficient penetration of
369 AMB (39, 40), while this has not yet been investigated in cryptococcoma models.
370 Preclinical studies using this model could help to optimize clinical treatment
371 strategies for cryptococcomas.

372 Our current study validated the use of *in vivo* imaging techniques for non-invasive
373 testing of treatment efficacy in various organs. It was not a direct aim of this proof-of-
374 concept study to identify the most optimal treatment regimens for cryptococcosis.
375 Accordingly, our study was sufficiently powered to demonstrate visually observable
376 treatment effects with statistical validity, but a larger number of animals would likely
377 be required for detecting potential more subtle effects. Our results indicated that the
378 applied monotherapy regimens were insufficient to effectively clear the infection from
379 all body sites. One reason for this limited efficacy of treatment can be attributed to the
380 late start of therapy, which was initiated when disease had already been manifested.
381 Such a limited efficacy of antifungal treatment has also been reported in other models
382 with delayed treatment (26, 41), and underlines the importance of early diagnosis
383 and rapid initiation of therapy (42, 43). Nonetheless, our results showed that *in vivo*
384 antifungal efficacy in various organs can largely be attributed to the known
385 biodistribution of the tested compounds. In the disseminated disease model, the
386 potent fungicidal drug L-AMB reduced the infection load in the kidney and eradicated
387 all cryptococci from the spleen, which is consistent with its high tissue concentration

388 in this organ (44, 45). This was in contrast to the brain, where the best results were
389 obtained using FLC, a drug that effectively crosses the BBB. I.p. injection with L-AMB
390 only mildly reduced brain fungal load, consistent with its low availability in the brain
391 which may hamper efficient control of CNS infections (15, 45). A higher treatment
392 efficacy in the brain could potentially be achieved by i.v. injection of L-AMB through
393 increased systemic uptake, although daily i.v. injections in mice are technically more
394 challenging. An earlier initiation, prolonged treatment or combination therapy with
395 different antifungals would likely also enhance treatment efficacy, and many different
396 combinations and regimens have previously been evaluated in animal studies and
397 clinical trials. Our proof-of-concept study shows that preclinical imaging is sensitive
398 enough to detect even small treatment effects. As such, this work can form the basis
399 for additional follow-up studies that search the most effective treatment strategy by
400 use of preclinical imaging in appropriately powered animal studies.

401 In conclusion, we have shown that BLI and MRI allow non-invasive evaluation of the
402 *in vivo* efficacy of antifungal compounds combatting CNS cryptococcosis. Both *in*
403 *vitro* and *in vivo* BLI allowed for the rapid real-time assessment of the viable fungal
404 load and its response to therapy, while treatment effects in multiple organs could be
405 evaluated simultaneously. MRI allowed monitoring of the spatial distribution and
406 growth rate of the brain lesions following antifungal treatment. The combination of
407 both techniques provided highly complementary information and allowed longitudinal
408 monitoring of the treatment effects in individual animals. This approach proved to be
409 a powerful tool that can reveal important aspects of the dynamics of treatment
410 response, which could be missed by single time point measurements like CFU and/or
411 survival analyses and potentially lead to misinterpretation of therapeutic drug
412 efficacy. Therefore, non-invasive *in vivo* imaging techniques have the potential to

413 help improve the efficiency and accuracy of preclinical drug testing for CNS infections
414 and accelerate the translation of promising drug candidates or treatment regimens to
415 the clinic.

416 **Material and methods**

417 **Fungal strains**

418 The bioluminescent *C. neoformans* KN99 α strain (28) expressing a red-shifted,
419 codon-optimized firefly luciferase was used for both *in vitro* and *in vivo* experiments.
420 Additional *in vitro* experiments were performed using a wild-type and red fluorescent
421 *C. neoformans* KN99 α strain, expressing the protein E2-Crimson (see supplementary
422 methods for construction of this strain). A GFP-expressing *C. neoformans* H99 strain
423 (46) was used for histology of the infected brains. All *Cryptococcus* strains were
424 cultured on Sabouraud agar (Bio-Rad, Temse, Belgium) for 2-3 days at 37°C (*in*
425 *vitro*) or 30°C (*in vivo* experiments) prior to transfer to liquid cultures.

426 ***In vitro* experiments**

427 *Bioluminescence assay of antifungal effects*

428 Liquid cultures were grown in DYP medium (1 % glucose, 0.5% yeast extract, 1%
429 peptone) for 24 hours at 37°C while shaking (200 rpm). Amphotericin B deoxycholate
430 (AMB-d, 0.1 mg/ml, Fungizone, Bristol-Myers Squibb, Utrecht, The Netherlands),
431 fluconazole (FLC, 0.5 mg/ml, TCI Europe, Zwijndrecht, Belgium) or an equal volume
432 of sterile water (control) was added to the culture. Both drugs were dissolved or
433 dispersed in sterile water. Cultures (10 ml) were incubated at 37°C while shaking and
434 samples were measured immediately after, 2, 4, 6, 8, 24, 48 and 72 hours after

435 addition of the antifungals. The results are expressed relative to the average signal
436 obtained immediately after addition of the drug to normalize for differences in initial
437 culture density.

438 *Temporal profile of bioluminescence after antifungal therapy*

439 Cultures were inoculated in liquid Sabouraud medium (Bio-Rad) and grown for 20
440 hours at 37°C while shaking. AMB-d, liposomal amphotericin B (L-AMB, AmbiSome,
441 Gilead Sciences, Carrigtohill, Ireland), FLC, natamycin (JK Scientific GmbH,
442 Pforzheim, Germany) or sodium dodecyl sulphate (SDS, Merck, Hohenbrunn,
443 Germany) were dissolved or suspended in sterile water. Antifungal compounds were
444 added to aliquots (4 ml) of the cultures at a final concentration of 0.01, 0.1, 1, 10 or
445 100 µg/ml, while SDS was used at 1, 0.1, 0.01, 0.001 and 0.0001 %. An equal
446 volume of sterile water was added to the no drug control. Bioluminescence was
447 measured at 5 minutes, 40 minutes, 1, 2, 4, 6, 8 and 26 hours after antifungal
448 addition.

449 *In vitro bioluminescence and fluorescence measurements*

450 100 µl of the culture was transferred to a 96-well plate (Falcon Microtest 96, Becton
451 Dickinson, Meylan Cedex, France) and 100 µl of D-luciferin (final concentration 0.15
452 µg/ml, in phosphate-buffered saline (PBS), Luciferin-EF, Promega, USA) was added.
453 Bioluminescence was measured in triplicate or quadruplicate samples using a plate
454 reader (Wallac Victor 1420, Perkin Elmer, Waltham, USA) with 10 seconds
455 measurement time. For assessment of fluorescent E2-Crimson strains, auto-
456 fluorescence and auto-luminescence, see supplementary methods.

457 ***In vivo experiments***

458 Animals were housed in individually ventilated cages and received water and
459 standard food ad libitum. Female BALB/c mice (internal stock KU Leuven or Charles
460 River Laboratories) were infected at an age of 9-10 weeks. All animal experiments
461 were conducted in accordance with European directive 2010/63/EU and approved by
462 the animal ethics committee of KU Leuven (P006/2017, P103/2012).

463 *Preparation of Cryptococcus neoformans inoculum*

464 The bioluminescent *C. neoformans* strain was cultured in liquid Sabouraud medium
465 for 2-3 days at 30°C. As previously described (28), fungal cells were harvested by
466 centrifugation, washed twice with Dulbecco's PBS (Gibco, Paisley, UK), counted
467 using a Neubauer counting chamber and diluted to the desired concentration in PBS.
468 The number of CFUs in the inoculum was confirmed by plating on Sabouraud agar.

469 *Experiment 1: Systemic treatment in the meningoencephalitis model (Fig. 3A)*

470 Animals were anaesthetized using 1.5-2% isoflurane (IsoVET®, Primal Critical Care
471 Limited, West Drayton, UK) in 100% oxygen and infected by tail vein injection of
472 50,000 fungal cells in 100 µl of PBS to induce disseminated infection and subsequent
473 meningoencephalitis (28). Starting from day 3 p.i., animals (n = 4 per group) received
474 antifungal treatment by i.p. injection of L-AMB (10 mg/kg), saline, or FLC (75 mg/kg).
475 For the latter, we initially aimed to administer 150 mg/kg (corresponding to 800
476 mg/day in humans) based on previous reports of high-dose FLC treatment (47), but
477 we found that this was not feasible due to the limited solubility of FLC in saline. L-
478 AMB was dispersed in sterile water and diluted with 5% glucose solution prior to
479 injection, as per the manufacturer's instructions. 1 animal in the FLC group did not
480 develop infection, most likely due to inefficient i.v. injection and was excluded from
481 the analysis. BLI scans were performed on day 3 (prior to antifungal treatment), 4, 5,

482 6 and 7, while 2D and 3D MRI scans were done on day 4 and 6. BLI was performed
483 prior to the daily dose of the antifungal, except on day 4.

484 *Experiment 2: Systemic treatment in the cryptococcoma model (Fig. 3B)*

485 Focal cryptococcal brain lesions were induced by intracranial stereotactic injection,
486 based on a previously described rat model (48). Mice were anaesthetized by i.p.
487 injection of ketamine (45-60 mg/kg, Nimatek®, Eurovet Animal Health, Bladel, The
488 Netherlands) and medetomidine (0.6-0.8 mg/kg, Domitor®, Orion Pharma, Espoo,
489 Finland). Fur on the head was clipped, the skin was disinfected and local analgesia
490 was administered (2% lidocaine, Linisol®, Braun, Berlin, Germany). The animal's
491 head was fixed in a stereotactic frame (Stoelting, Wood Dale, IL, USA) and 10,000
492 bioluminescent *Cryptococcus* cells were injected (1 µl, rate of 0.5 µl/min) in the
493 striatum using a 10 µl Hamilton syringe with 30 gauge needle (Hamilton Company,
494 Reno, NV, USA). Injection coordinates were 0.5 mm anterior and 2 mm lateral to
495 bregma, and 3 mm from the dura. To prevent backflow of the injected cells, the burr
496 hole was closed using dental filling resin (NanoFil® flowable light curing composite,
497 AT&M Biomaterials, Beijing, China). The incision site was sutured and anesthesia
498 was reversed by i.p. injection of atipamezole hydrochloride (0.5 mg/kg, Antisedan®,
499 Orion Pharma). Additional animals were injected with a GFP-expressing *C.*
500 *neoformans* H99 strain for histological analysis of the cryptococcoma model (see
501 supplementary methods).

502 Starting from day 3 p.i., mice (n = 4 per group) received daily i.p. injections with
503 saline, L-AMB (10 mg/kg) or FLC (75 mg/kg). A fourth group of animals received a
504 single high dose of L-AMB (20 mg/kg) i.v., based on previous reports on the efficacy
505 of this regimens (49). BLI and 2D MRI scans were performed on day 3 (prior to
506 antifungal treatment), 6 and 9 p.i..

507 *Experiment 3: Intracerebral treatment in the cryptococcoma model (Fig. 3C)*

508 Focal cryptococcal brain lesions were induced by stereotactic injection. On day 6 and
509 8 p.i., mice (n = 5) received an intracranial stereotactic injection of L-AMB (2.5 µl of
510 0.6 mg/ml in sterile water) inside the brain lesion, at the same coordinates as used
511 for induction. 2.5 µl was distributed in five steps of 0.5 µl, spaced every 0.5 mm
512 between 4 and 2 mm from the dura. Control animals (n = 4) were injected with 2.5 µl
513 of sterile water. Mice were scanned using BLI and MRI (2D) on day 6 (prior to the first
514 treatment), 8 and 10.

515 **Image acquisition and analysis**

516 *BLI*

517 Mice were injected i.p. with D-luciferin solution (15 mg/ml) at a dose of 126 mg/kg
518 prior to anesthesia (50). Immediately afterwards, animals were anaesthetized using
519 1.5-2% isoflurane in 100% oxygen. Ten to fifteen minutes after D-luciferin injection,
520 mice were placed in prone position in an IVIS Spectrum imaging system (Perkin
521 Elmer) equipped with Living Image Software (version 4.5.2). Consecutive images
522 were acquired during 30 minutes using an exposure time of 1 minute, F/stop 1,
523 subject height of 1.5 cm and medium binning. The total photon flux was quantified
524 using Living Image Software (version 4.5.4). Regions of interest were located in the
525 brain (cryptococcoma model: circular ROI of 1.8 cm diameter, meningoencephalitis
526 model: rectangular ROI of 1.6 by 1.3 cm) or upper abdomen (including spleen and
527 kidney region, 2.5 by 1.3 cm). Per animal and time point, the highest total photon flux
528 obtained from all consecutive images was used for further statistical analysis.

529 *Magnetic resonance imaging*

530 MR scans were acquired using a 9.4T preclinical MRI scanner with 20 cm bore
531 (Biospec 94/20) and a linearly polarized resonator (72 mm diameter) in combination
532 with an actively decoupled mouse brain surface coil (all Bruker Biospin, Ettlingen,
533 Germany). A physiological monitoring system (Small Animal Instruments Inc., Stony
534 Brook, NY, US) was used to monitor the animals' breathing rate and body
535 temperature during isoflurane anesthesia. After acquisition of localizer images, a 2D
536 coronal T₂-weighted MR brain scan was acquired with the following parameters: spin-
537 echo sequence, RARE factor of 8, TR/effective TE 4200/36.3 ms, field of view 2 x 1.5
538 cm, 12 slices with 0.5 mm slice thickness, 100 μm in plane resolution and a scan
539 time of 1 min. A 2D axial brain scan was acquired with a RARE factor of 8,
540 TR/effective TE 4200/36.3 ms, field of view 2 x 2 cm, 9 slices with 0.5 mm thickness
541 and 0.2 mm slice gap, in plane resolution of 78.125 μm and a scan time of 1.66 min.
542 Parameters for the 3D T₂-weighted brain MR scans (meningoencephalitis model)
543 were: spin-echo sequence, RARE factor 10, TR/TE 1000/36 ms, FOV 2.4×1.5×0.83
544 cm, isotropic spatial resolution of approximately 94 μm and a scan time of 15 min.

545 Lesions were manually delineated on the 2D or 3D scans using the brush tool in ITK-
546 SNAP (version 3.4.0, (51)). The reported lesion volume in the cryptococcoma model
547 is the average volume obtained from the coronal and axial 2D scans. For the 3D
548 scans in the meningoencephalitis model, the number of brain lesions and average
549 volume per lesion was determined in ImageJ (version 1.49, National Institute of
550 Health, USA, (52)) by using the 3D object counter (53) after applying a Watershed
551 algorithm on the segmentation image.

552 **CFU analysis**

553 After the last imaging session, or when humane endpoints were reached, animals
554 were sacrificed by i.p. injection of a pentobarbital overdose. The brains were isolated,

555 weighted and homogenized after addition of PBS. Serial 10-fold dilutions were plated
556 in triplicate on Sabouraud agar. After 3 days incubation at room temperature or 2
557 days at 30°C, the number of colonies was counted manually. All reported CFU
558 counts are expressed as CFUs/g weighted tissue. For correlations with the imaging
559 data, animals that succumbed to disease prior to the end of the experiments were
560 excluded.

561 **Statistical analysis**

562 Data were analyzed using Graphpad Prism (version 8.1.2). Time-kill curves were
563 analyzed using a two-way repeated measures ANOVA, followed by a Dunnett's post-
564 test to compare each treatment group to the control curve. *In vitro* data at specific
565 time points were analyzed using a one-way ANOVA with Dunnett's post-test
566 compared to the control setting.

567 Longitudinal *in vivo* imaging datasets were analyzed using a mixed-effects model
568 with Geisser-Greenhouse correction to investigate whether treatment effects were
569 significant. If no significant effect was found, only this p-value is reported. When
570 treatment was a significant factor, p-values for the comparison of specific treatment
571 groups to the control group (over all time points) are reported after using a Dunnett's
572 post-test. This was followed by a second Dunnett's post-test comparing the groups at
573 the specific time points (significance indicated on the graph). CFU data was analyzed
574 using an unpaired t-test or one-way ANOVA with Dunnett's post-test and linear
575 regression with Pearson correlation coefficients. *In vivo* BLI and CFU data were log-
576 transformed prior to statistical analysis.

577 **Acknowledgements**

578 The authors wish to thank Jens Wouters and Sarah Belderbos for their assistance
579 and thank Dr. Kristof Govaerts for his guidance with the MRI quantification. We
580 gratefully acknowledge Dr. Steffen Fieuws (L-BioStat, KU Leuven) for statistical
581 advice. This work was funded by the European ERA-NET project 'CryptoView' (3rd
582 call of the FP7 program Infect-ERA), the Research Foundation-Flanders (FWO,
583 1506114N) and KU Leuven (PF 10/017 (IMIR), CREA/14/015). L.V. is a PhD fellow
584 strategic basic research at the FWO (151313). J.P. received a PhD grant for strategic
585 basic research from the Agency for Innovation by Science and Technology (IWT,
586 141230). G.V.V. received a postdoctoral fellowship from the FWO (12N7615N).

587 **Competing interests**

588 Katrien Lagrou received consultancy fees from Pfizer, Abbott, MSD and SMB
589 Laboratoires Brussels, she received travel support from Pfizer and MSD and speaker
590 fees from Gilead, MSD, Roche, Abbott; all outside the submitted work.

591 **References**

- 592 1. Góralaska K, Blaszkowska J, Dzikowiec M. 2018. Neuroinfections caused by fungi. *Infection*
593 46:443–459.
- 594 2. Schwartz S, Kontoyiannis DP, Harrison T, Ruhnke M. 2018. Advances in the diagnosis and
595 treatment of fungal infections of the CNS. *Lancet Neurol* 17:362–372.
- 596 3. Enoch DA, Yang H, Aliyu SH, Micallef C. 2017. The Changing Epidemiology of Invasive Fungal
597 Infections, p. 17–65. *In* . Humana Press, New York, NY.
- 598 4. Lee SC, Dickson DW, Casadevall A. 1996. Pathology of cryptococcal meningoencephalitis:
599 Analysis of 27 patients with pathogenetic implications. *Hum Pathol* 27:839–847.
- 600 5. Williamson PR, Jarvis JN, Panackal AA, Fisher MC, Molloy SF, Loyse A, Harrison TS.
601 Cryptococcal meningitis: epidemiology, immunology, diagnosis and therapy. *Nat Rev Neurol*
602 13:13–24.
- 603 6. Chen S, Sorrell T, Nimmo G, Speed B, Currie B, Ellis D, Marriott D, Pfeiffer T, Parr D, Byth K.
604 2000. Epidemiology and Host- and Variety-Dependent Characteristics of Infection Due to
605 *Cryptococcus neoformans* in Australia and New Zealand. *Clin Infect Dis* 31:499–508.
- 606 7. Nguyen MH, Husain S, Clancy CJ, Peacock JE, Hung C-C, Kontoyiannis DP, Morris AJ, Heath
607 CH, Wagener M, Yu VL. 2010. Outcomes of central nervous system cryptococcosis vary with
608 host immune function: Results from a multi-center, prospective study. *J Infect* 61:419–426.
- 609 8. Roemer T, Krysan DJ. 2014. Antifungal drug development: challenges, unmet clinical needs,
610 and new approaches. *Cold Spring Harb Perspect Med* 4:a019703.
- 611 9. Perfect JR. 2017. The antifungal pipeline: a reality check. *Nat Rev Drug Discov* 16:603–616.
- 612 10. Sloan D, Parris V. 2014. Cryptococcal meningitis: epidemiology and therapeutic options. *Clin*
613 *Epidemiol* 6:169.
- 614 11. World Health Organization. 2018. Guidelines for the diagnosis, prevention and management of
615 cryptococcal disease in HIV-infected adults, adolescents and children: supplement to the 2016
616 consolidated guidelines on the use of antiretroviral drugs for treating and preventing HIV
617 infection. Who.
- 618 12. Sloan DJ, Dedicoat MJ, Laloo DG. 2009. Treatment of cryptococcal meningitis in resource
619 limited settings. *Curr Opin Infect Dis* 22:455–63.
- 620 13. Molloy SF, Kanyama C, Heyderman RS, Loyse A, Kouanfack C, Chanda D, Mfinanga S,

- 621 Temfack E, Lakhi S, Lesikari S, Chan AK, Stone N, Kalata N, Karunaharan N, Gaskell K, Peirse
622 M, Ellis J, Chawinga C, Lontsi S, Ndong J-G, Bright P, Lupiya D, Chen T, Bradley J, Adams J,
623 van der Horst C, van Oosterhout JJ, Sini V, Mapoure YN, Mwaba P, Bicanic T, Lalloo DG,
624 Wang D, Hosseinipour MC, Lortholary O, Jaffar S, Harrison TS. 2018. Antifungal Combinations
625 for Treatment of Cryptococcal Meningitis in Africa. *N Engl J Med* 378:1004–
626 1017.
- 627 14. Krysan DJ. 2015. Toward improved anti-cryptococcal drugs: Novel molecules and repurposed
628 drugs. *Fungal Genet Biol* 78:93–98.
- 629 15. Felton T, Troke PF, Hope WW. 2014. Tissue penetration of antifungal agents. *Clin Microbiol*
630 *Rev* 27:68–88.
- 631 16. Capilla J, Clemons K V., Stevens DA. 2007. Animal models: an important tool in mycology.
632 *Med Mycol* 45:657–684.
- 633 17. Hohl TM. 2014. Overview of vertebrate animal models of fungal infection. *J Immunol Methods*
634 410:100–12.
- 635 18. Avci P, Karimi M, Sadasivam M, Antunes-Melo WC, Carrasco E, Hamblin MR. 2018. *In-vivo*
636 monitoring of infectious diseases in living animals using bioluminescence imaging. *Virulence*
637 9:28–63.
- 638 19. Vande Velde G, Kucharíková S, Van Dijck P, Himmelreich U. 2018. Bioluminescence imaging
639 increases in vivo screening efficiency for antifungal activity against device-associated *Candida*
640 *albicans* biofilms. *Int J Antimicrob Agents* 52:42–51.
- 641 20. Persyn A, Rogiers O, Brock M, Vande Velde G, Lamkanfi M, Jacobsen ID, Himmelreich U,
642 Lagrou K, Van Dijck P, Kucharíková S. 2019. Monitoring of Fluconazole and Caspofungin
643 Activity against In Vivo *Candida glabrata* Biofilms by Bioluminescence Imaging. *Antimicrob*
644 *Agents Chemother* 63.
- 645 21. Vande Velde G, Kucharíková S, Schrevels S, Himmelreich U, Van Dijck P. 2014. Towards
646 non-invasive monitoring of pathogen-host interactions during *Candida albicans* biofilm
647 formation using in vivo bioluminescence. *Cell Microbiol* 16:115–30.
- 648 22. Brock M, Jouvion G, Droin-Bergère S, Dussurget O, Nicola M-A, Ibrahim-Granet O. 2008.
649 Bioluminescent *Aspergillus fumigatus*, a new tool for drug efficiency testing and in vivo
650 monitoring of invasive aspergillosis. *Appl Environ Microbiol* 74:7023–35.

- 651 23. Galiger C, Brock M, Jouvion G, Savers A, Parlato M, Ibrahim-Granet O. 2013. Assessment of
652 efficacy of antifungals against *Aspergillus fumigatus*: value of real-time bioluminescence
653 imaging. *Antimicrob Agents Chemother* 57:3046–59.
- 654 24. Kaskova ZM, Tsarkova AS, Yampolsky I V. 2016. 1001 lights: Luciferins, luciferases, their
655 mechanisms of action and applications in chemical analysis, biology and medicine. *Chem Soc*
656 *Rev. Royal Society of Chemistry*.
- 657 25. Binder U, Navarro-Mendoza MI, Naschberger V, Bauer I, Nicolas FE, Pallua JD, Lass-Flörl C,
658 Garre V, Binder U, Navarro-Mendoza MI, Naschberger V, Bauer I, Nicolas FE, Pallua JD, Lass-
659 Flörl C, Garre V. 2018. Generation of A *Mucor circinelloides* Reporter Strain—A Promising New
660 Tool to Study Antifungal Drug Efficacy and Mucormycosis. *Genes (Basel)* 9:613.
- 661 26. Poelmans J, Himmelreich U, Vanherp L, Zhai L, Hillen A, Holvoet B, Belderbos S, Brock M,
662 Maertens J, Vande Velde G, Lagrou K. 2018. A Multimodal Imaging Approach Enables *In Vivo*
663 Assessment of Antifungal Treatment in a Mouse Model of Invasive Pulmonary Aspergillosis.
664 *Antimicrob Agents Chemother* 62:AAC.00240-18.
- 665 27. Jacobsen ID, Lüttich A, Kurzai O, Hube B, Brock M. 2014. In vivo imaging of disseminated
666 murine *Candida albicans* infection reveals unexpected host sites of fungal persistence during
667 antifungal therapy. *J Antimicrob Chemother* 69:2785–2796.
- 668 28. Vanherp L, Ristani A, Poelmans J, Hillen A, Lagrou K, Janbon G, Brock M, Himmelreich U,
669 Vande Velde G. 2019. Sensitive bioluminescence imaging of fungal dissemination to the brain
670 in mouse models of cryptococcosis. *Dis Model Mech* 12:dmm039123.
- 671 29. Dorsaz S, Coste AT, Sanglard D. 2017. Red-Shifted Firefly Luciferase Optimized for *Candida*
672 *albicans* *In vivo* Bioluminescence Imaging. *Front Microbiol* 8:1478.
- 673 30. Palacios DS, Dailey I, Siebert DM, Wilcock BC, Burke MD. 2011. Synthesis-enabled functional
674 group deletions reveal key underpinnings of amphotericin B ion channel and antifungal
675 activities. *Proc Natl Acad Sci* 108:6733–6738.
- 676 31. Bolard J. 1986. How do the polyene macrolide antibiotics affect the cellular membrane
677 properties? *Biochim Biophys Acta* 864:257–304.
- 678 32. Virta M, Åkerman KEO, Saviranta P, Oker-Blom C, Karp MT. 1995. Real-time measurement of
679 cell permeabilization with low-molecular-weight membranolytic agents. *J Antimicrob Chemother*
680 36:303–315.

- 681 33. te Welscher YM, ten Napel HH, Balagué MM, Souza CM, Riezman H, de Kruijff B, Breukink E.
682 2008. Natamycin blocks fungal growth by binding specifically to ergosterol without
683 permeabilizing the membrane. *J Biol Chem* 283:6393–401.
- 684 34. Van Dijck P, Sjollem J, Cammue BP, Lagrou K, Berman J, d'Enfert C, Andes DR, Arendrup
685 MC, Brakhage AA, Calderone R, Cantón E, Coenye T, Cos P, Cowen LE, Edgerton M, Espinel-
686 Ingroff A, Filler SG, Ghannoum M, Gow NAR, Haas H, Jabra-Rizk MA, Johnson EM, Lockhart
687 SR, Lopez-Ribot JL, Maertens J, Munro CA, Nett JE, Nobile CJ, Pfaller MA, Ramage G,
688 Sanglard D, Sanguinetti M, Spriet I, Verweij PE, Warris A, Wauters J, Yeaman MR, Zaat SAJ,
689 Thevissen K. 2018. Methodologies for in vitro and in vivo evaluation of efficacy of antifungal
690 and antibiofilm agents and surface coatings against fungal biofilms. *Microb cell (Graz, Austria)*
691 5:300–326.
- 692 35. Ayzenberg I, Schlevogt S, Metzdorf J, Stahlke S, Pedreitturia X, Hunfeld A, Couillard-Despres
693 S, Kleiter I. 2015. Analysis of Neurogenesis during Experimental Autoimmune
694 Encephalomyelitis Reveals Pitfalls of Bioluminescence Imaging. *PLoS One* 10:e0118550.
- 695 36. Hospenthal DR, Bennett JE. 2000. Persistence of Cryptococcomas on Neuroimaging. *Clin*
696 *Infect Dis* 31:1303–1306.
- 697 37. Perfect JR, Dismukes WE, Dromer F, Goldman DL, Graybill JR, Hamill RJ, Harrison TS,
698 Larsen RA, Lortholary O, Nguyen M-H, Pappas PG, Powderly WG, Singh N, Sobel JD, Sorrell
699 TC. 2010. Clinical practice guidelines for the management of cryptococcal disease: 2010
700 update by the infectious diseases society of america. *Clin Infect Dis* 50:291–322.
- 701 38. Ulett KB, Cockburn JWJ, Jeffree R, Woods ML. 2017. Cerebral cryptococcoma mimicking
702 glioblastoma. *BMJ Case Rep* 2017.
- 703 39. Pai MP, Sakoglu U, Peterson SL, Lyons CR, Sood R. 2009. Characterization of BBB
704 permeability in a preclinical model of cryptococcal meningoencephalitis using magnetic
705 resonance imaging. *J Cereb Blood Flow Metab* 29:545–53.
- 706 40. Takemoto K, Yamamoto Y, Ueda Y. 2006. Influence of the Progression of Cryptococcal
707 Meningitis on Brain Penetration and Efficacy of AmBisome in a Murine Model. *Chemotherapy*
708 52:271–278.
- 709 41. Lu R, Hollingsworth C, Qiu J, Wang A, Hughes E, Xin X, Konrath KM, Elsegeiny W, Park Y-D,
710 Atakulu L, Craft JC, Tramont EC, Mannino R, Williamson PR. 2019. Efficacy of Oral

- 711 Enochleated Amphotericin B in a Mouse Model of Cryptococcal Meningoencephalitis. *MBio*
712 10:e00724-19.
- 713 42. Pasquier E, Kunda J, De Beaudrap P, Loyse A, Temfack E, Molloy SF, Harrison TS, Lortholary
714 O. 2018. Long term mortality and disability in Cryptococcal Meningitis: a systematic literature
715 review. *Clin Infect Dis* 66:1122–1132.
- 716 43. Aye C, Henderson A, Yu H, Norton R. 2016. Cryptococcosis: the impact of delay to diagnosis.
717 *Clin Microbiol Infect* 22:632–635.
- 718 44. Bellmann R, Smuszkiewicz P. 2017. Pharmacokinetics of antifungal drugs: practical
719 implications for optimized treatment of patients. *Infection* 45:737.
- 720 45. Vogelsinger H, Weiler S, Djanani A, Kountchev J, Bellmann-Weiler R, Wiedermann CJ,
721 Bellmann R. 2006. Amphotericin B tissue distribution in autopsy material after treatment with
722 liposomal amphotericin B and amphotericin B colloidal dispersion. *J Antimicrob Chemother*
723 57:1153–1160.
- 724 46. Voelz K, Johnston SA, Rutherford JC, May RC. 2010. Automated analysis of cryptococcal
725 macrophage parasitism using GFP-tagged cryptococci. *PLoS One* 5:e15968.
- 726 47. Santos JRA, Ribeiro NQ, Bastos RW, Holanda RA, Silva LC, Queiroz ER, Santos DA. 2017.
727 High-dose fluconazole in combination with amphotericin B is more efficient than monotherapy
728 in murine model of cryptococcosis. *Sci Rep* 7:4661.
- 729 48. Himmelreich U, Dzendrowskyj TE, Allen C, Dowd S, Malik R, Shehan BP, Russell P, Mountford
730 CE, Sorrell TC. 2001. Cryptococcomas distinguished from gliomas with MR spectroscopy: an
731 experimental rat and cell culture study. *Radiology* 220:122–8.
- 732 49. Lestner J, McEntee L, Johnson A, Livermore J, Whalley S, Schwartz J, Perfect JR, Harrison T,
733 Hope W. 2017. Experimental Models of Short Courses of Liposomal Amphotericin B for
734 Induction Therapy for Cryptococcal Meningitis. *Antimicrob Agents Chemother* 61:e00090-17.
- 735 50. Aswendt M, Adamczak J, Couillard-Despres S, Hoehn M, Bailly C, Gaensler K. 2013. Boosting
736 Bioluminescence Neuroimaging: An Optimized Protocol for Brain Studies. *PLoS One* 8:e55662.
- 737 51. Yushkevich PA, Piven J, Hazlett HC, Smith RG, Ho S, Gee JC, Gerig G. 2006. User-guided 3D
738 active contour segmentation of anatomical structures: Significantly improved efficiency and
739 reliability. *Neuroimage* 31:1116–1128.
- 740 52. Schneider CA, Rasband WS, Eliceiri KW. 2012. NIH Image to ImageJ: 25 years of image

741 analysis. *Nat Methods* 9:671–675.

742 53. Bolte S, Cordelières FP. 2006. A guided tour into subcellular colocalization analysis in light
743 microscopy. *J Microsc* 224:213–232.

Figure legends

744 **Figure 1: *In vitro* bioluminescence assay of antifungal effects.** Amphotericin B
745 deoxycholate (AMB-d, 0.1 mg/ml), fluconazole (FLC, 0.5 mg/ml), or sterile water
746 (control) were added to pre-grown (24 h old) liquid cultures. Bioluminescence was
747 measured immediately after, 2, 4, 6, 8, 24, 48 and 72 hours after antifungal addition
748 by adding D-luciferin (0.15 µg/ml) to samples of the culture. The bioluminescence
749 signal is expressed relative to the signal obtained immediately after addition of
750 antifungal (0 h). Curves were significantly different for AMB-d ($p < 0.0001$) and
751 fluconazole ($p = 0.0152$) compared to the control curve. Two-way repeated measures
752 ANOVA with Dunnett's multiple comparison post-test. Graph shows mean \pm SD.

753 **Figure 2: Temporal profile of the bioluminescence signals in response to**
754 **different antifungal compounds.** Bioluminescent *C. neoformans* cells in liquid
755 culture (20 h old) were exposed to various doses of antifungals and the
756 bioluminescence was measured in real time at the indicated time points by adding D-
757 luciferin to culture samples. A) Amphotericin B deoxycholate (AMB-d) showed a
758 dose-dependent antifungal effect. Bioluminescence increased transiently shortly after
759 addition. B) Liposomal amphotericin B (L-AMB) induced a similar but more delayed
760 response. C) Fluconazole showed a modest antifungal effect at the tested
761 concentrations. D) Exposure to natamycin induced a dose-dependent killing of the
762 fungi. A transient increase was only observed for the highest concentration tested. E)
763 Sodium dodecyl sulphate (SDS) caused a rapid dose-dependent decrease in
764 bioluminescence. Graphs show mean \pm SD.

765 **Figure 3: Experimental set-ups for *in vivo* imaging of treatment efficacy in**
766 **delayed-treatment models.** A) Systemic treatment in the model of
767 meningoencephalitis following disseminated disease. B) Systemic treatment in the
768 cryptococcoma model. C) Intracerebral treatment in the cryptococcoma model.
769 Abbreviations: i.cr.: intracranial; i.p.: intraperitoneal; i.v.: intravenous; BL: baseline
770 scans to assess infection status prior to initiation of treatment.

771 **Figure 4: BLI of antifungal treatment efficacy in a model of cryptococcal**
772 **meningoencephalitis.** Animals (n = 4 per group) were intravenously injected with
773 50,000 bioluminescent *C. neoformans* cells and received daily injections with saline,
774 liposomal amphotericin B (L-AMB, 10 mg/kg) or fluconazole (FLC, 75 mg/kg) starting
775 from day 3 p.i.. One animal in the FLC group did not have an established infection
776 and was excluded from further analysis (indicated with * on the images and with grey
777 dashed line on the graphs). A) BLI for the individual animals. B) Quantification of the
778 total photon flux in the brain region. The curves of FLC treated animals were
779 significantly different from the saline group ($p=0.016$), but not for L-AMB treated
780 animals ($p=0.7376$). On day 4, animals were injected with L-AMB shortly before BLI
781 acquisition, leading to a significantly increased bioluminescence. C) The total photon
782 flux in the abdominal region was significantly lower in the L-AMB group compared to
783 the saline group ($p=0.0001$), but not for the FLC group ($p=0.4374$). Graphs show
784 individual data points, mixed-effects model statistics with Dunnett's post-test. (-)
785 indicates that animals were lost to follow-up.

786 **Figure 5: Brain MRI after antifungal treatment in the meningoencephalitis**
787 **model.** Daily antifungal treatment with liposomal amphotericin B (L-AMB, 10 mg/kg),
788 fluconazole (FLC, 75 mg/kg) or saline (n = 4 each) was initiated 3 days after
789 intravenous injection with 50,000 *C. neoformans* cells. A) Slice of the 2D coronal MR
790 images for the individual animals (1 slice / animal). B) The total lesion volume
791 quantified from 3D MR images showed a significant effect for FLC-treatment
792 (p=0.0066) but not for L-AMB (p=0.2095). C). Treatment did not have a significant
793 effect (p=0.8561) on the number of lesions. D) The average lesion volume was
794 significantly lower in the FLC-treated animals (p=0.0007), but not in animals receiving
795 L-AMB treatment (p=0.9740). Graphs show individual data points, mixed-effects
796 model statistics with Dunnett's post-test. (-) indicates animals lost to follow-up, *
797 indicates one animal with unsuccessful induction of infection.

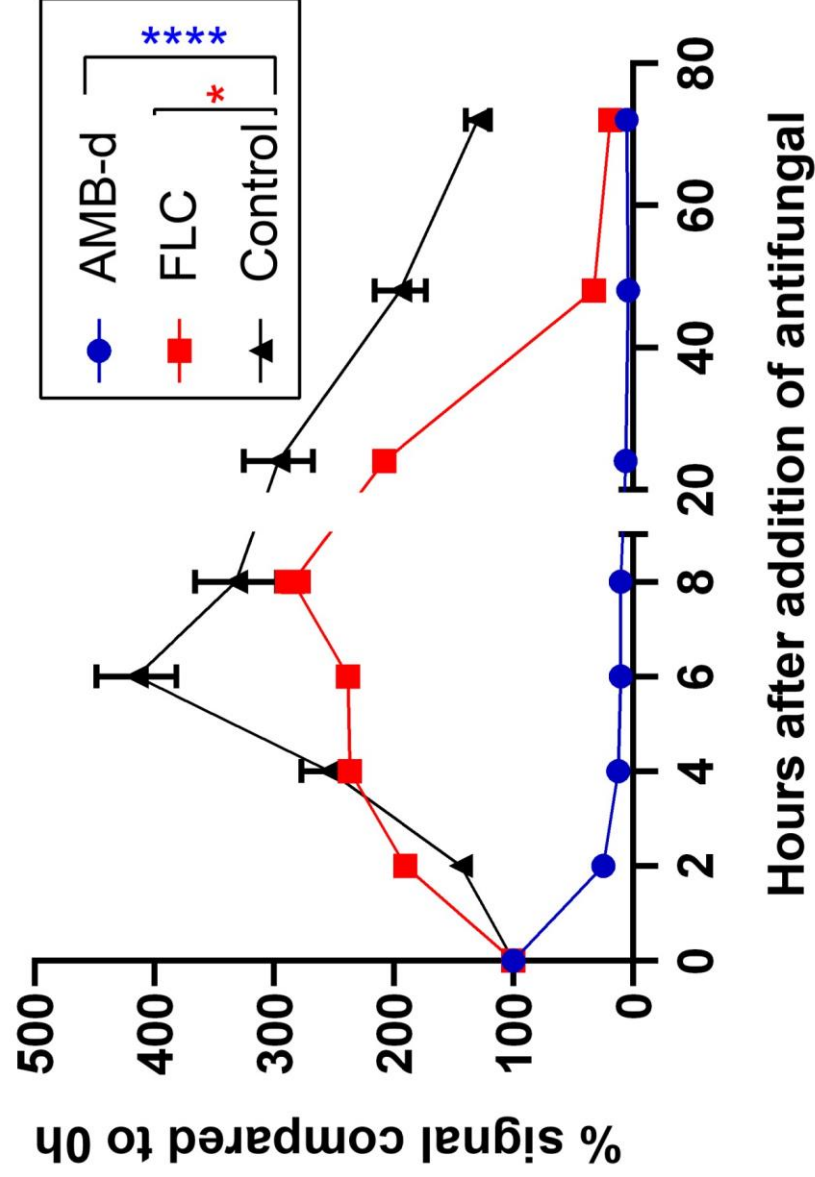
798 **Figure 6: CFU analysis of the brain, spleen and kidneys after antifungal**
799 **treatment in the meningoencephalitis model.** Disseminated infection was induced
800 by intravenous injection of 50,000 *C. neoformans* cells. Fungal load analysis was
801 performed after the last imaging session or when animals were sacrificed for humane
802 endpoints. A) Liposomal amphotericin B (L-AMB) and fluconazole (FLC) treatment
803 induced a small reduction in the fungal load in the brain (p=0.0103 and p=0.0054,
804 respectively). B) FLC treatment reduced the fungal load in the spleen (p=0.0128),
805 while for L-AMB no fungal cells could be recovered (p<0.0001). C) L-AMB and FLC
806 treatment lowered the fungal load in the kidneys (p<0.0001 and p=0.0023,
807 respectively). Graphs show mean \pm SD, one-way ANOVA with Dunnett's post-test.

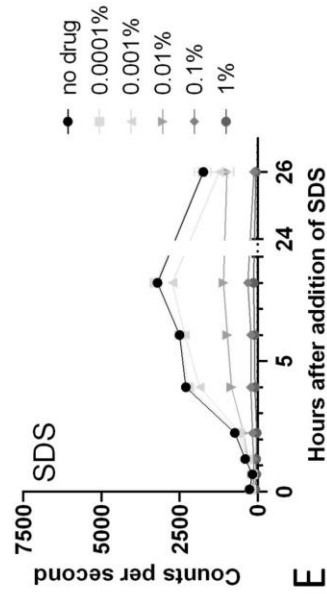
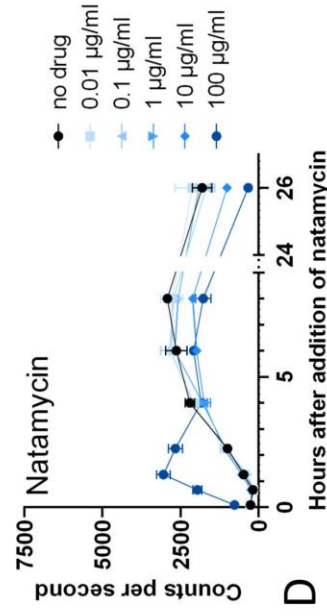
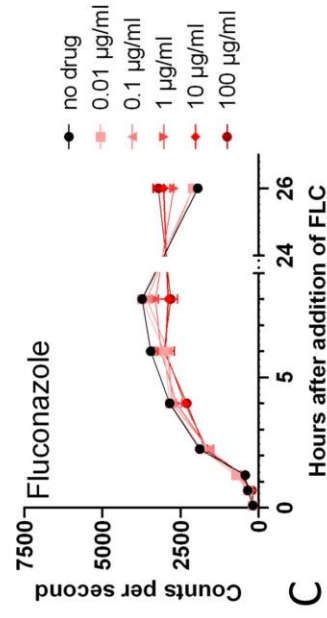
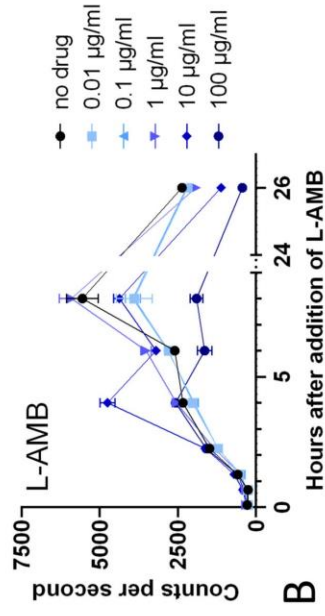
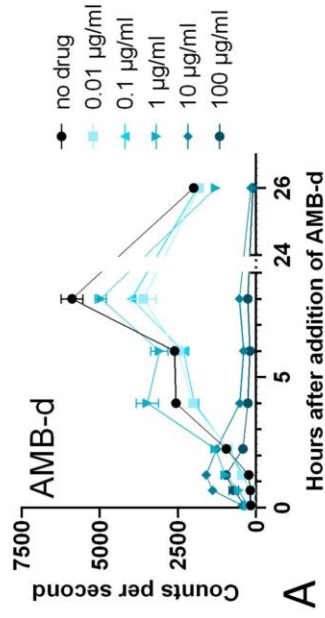
808 **Figure 7: BLI and MRI of antifungal treatment efficacy following systemic**
809 **treatment in the cryptococcoma model.** Focal cryptococcomas were induced by
810 stereotactic injection of 10,000 bioluminescent *C. neoformans* cells. Treatment (n=4
811 per group) was initiated on day 3 by daily i.p. injection of fluconazole (FLC, 75 mg/kg)
812 or liposomal amphotericin B (L-AMB, 10 mg/kg), or a single i.v. dose (20 mg/kg) of L-
813 AMB was given on day 3. A) BLI of treated animals. B) Coronal MRI slices for the
814 corresponding animals (1 slice per animal). C) Quantification of the BLI signal in the
815 brain region. Statistics did not show an overall significant effect of treatment
816 (p=0.2977). D) Lesion volume quantified from the MR images showed an overall
817 significant effect of treatment (p=0.0354), but no significant differences between the
818 saline and treatment groups. Animals with higher bioluminescence and MRI-based
819 evidence of cryptococcomas invading the ventricle are indicated with (*) on the
820 images and open symbols on the graphs. Graphs show individual data points, mixed-
821 effect model statistics with Dunnett's post-test. (-) indicates that animals were lost to
822 follow-up.

823 **Figure 8: CFU analysis of the brains after systemic treatment in the**
824 **cryptococcoma model and correlation with imaging readouts.** A) Treatment
825 induced a small but not significant decrease in the fungal brain load in animals
826 treated daily with fluconazole (FLC) or liposomal amphotericin B (L-AMB). No
827 significant differences were found (overall p-value = 0.0816). The animal with the
828 notably higher brain fungal load in the L-AMB groups displayed spreading of the
829 infection towards the forebrain. B-C) Quantification of *in vivo* BLI (B) and lesion
830 volume obtained from MRI (C) correlated well with the fungal burden in the brain.
831 When animals with spreading of the cryptococcomas to the ventricles (open symbols,
832 see Fig. 7) were excluded, the correlation of BLI and CFU results was strengthened
833 ($r= 0.7491$, $p=0.0050$). Graphs show data from individual animals. One-way ANOVA
834 with Dunnett's post-test or Pearson correlation coefficients with linear regression and
835 95% confidence bands.

836 **Figure 9: BLI and MRI of intracerebral treatment of cryptococcomas.** Animals
837 were stereotactically injected with 10,000 *C. neoformans* cells and liposomal
838 amphotericin B (L-AMB) (n = 5) or sterile water (n = 4) was injected inside the brain
839 lesion on day 6 and 8 p.i.. A) BLI of the infected animals on day 6 (before treatment),
840 8 and 10 p.i. B) Slice of the coronal 2D brain MRI for the same animals, showing a
841 small hyperintense region in the lesion at the site of injection (red arrows). C)
842 Quantification of the bioluminescence from the brain. D) Quantification of the lesion
843 volume on MRI. No significant effect of the treatment was found for the BLI or MRI
844 results at group level ($p=0.2725$ and $p=0.4396$, respectively). Numbers on the graphs
845 correspond to the specific animals on the images. Graphs show individual data

846 points, mixed-effect model statistics with Dunnett's post-test. (-) indicates that
847 animals were lost to follow-up.





A) Systemic treatment meningoencephalitis model

Mouse model	i.v. injection 50,000 bioluminescent <i>C. neoformans</i> cells	Treatment	Days post infection						
			n =	3	4	5	6	7	
Meningo-encephalitis model following disseminated disease	i.v. injection 50,000 bioluminescent <i>C. neoformans</i> cells	▪ Liposomal AMB 10 mg/kg, i.p.	4						
		▪ Fluconazole 75 mg/kg, i.p.	4						
		▪ Control: saline i.p.	4						
		BLI	✓ ^{BL}	✓	✓	✓	✓	✓	
		MRI		✓					

B) Systemic treatment cryptococcoma model

Mouse model	Intracranial injection (i.cr.) 10,000 bioluminescent <i>C. neoformans</i> cells	Treatment	Days post infection							
			n =	3	4	5	6	7	8	9
Cryptococcoma model	Intracranial injection (i.cr.) 10,000 bioluminescent <i>C. neoformans</i> cells	▪ Liposomal AMB 10 mg/kg, i.p.	4							
		▪ Fluconazole 75 mg/kg, i.p.	4							
		▪ Control: saline i.p.	4							
		Liposomal AMB 20 mg/kg, i.v.	4							
		BLI & MRI		✓ ^{BL}		✓			✓	

C) Intracerebral treatment cryptococcoma model

Mouse model	i.cr. injection 10,000 bioluminescent <i>C. neoformans</i> cells	Treatment	Days post infection								
			n =	3	4	5	6	7	8	9	10
Cryptococcoma model	i.cr. injection 10,000 bioluminescent <i>C. neoformans</i> cells	▪ Liposomal AMB 2.5 µl of 0.6 mg/ml, i.cr.	5								
		▪ Control: sterile water 2.5 µl i.cr.	4								
				BLI & MRI				✓ ^{BL}	✓		

